OPEN ACCESS
IOP Publishing
Journal of Physics D: Applied Physics
J. Phys. D: Appl. Phys. **52** (2019) 034001 (15pp)
https://doi.org/10.1088/1361-6463/aae752

Self-healing dyes for super-resolution fluorescence microscopy

Jasper H M van der Velde[1,5], Jochem H Smit[1,5], Elke Hebisch[2,3], Michiel Punter[1] and Thorben Cordes[1,4,6]

[1] Molecular Microscopy Research Group, Zernike Institute for Advanced Materials, University of Groningen, Nijenborgh 4, 9747 AG Groningen, The Netherlands
[2] Department of NanoBiophotonics, Max-Planck Institute for Biophysical Chemistry, Am Fassberg 11, 37077 Göttingen, Germany
[3] Division of Solid State Physics, Lund University, PO Box 118, SE-22100 Lund, Sweden
[4] Physical and Synthetic Biology, Faculty of Biology, Ludwig-Maximilians-Universität München, Großhadernerstr. 2-4, 82152 Planegg-Martinsried, Germany

E-mail: cordes@bio.lmu.de

Received 20 July 2018, revised 18 September 2018
Accepted for publication 10 October 2018
Published 7 November 2018

Abstract

In recent years, optical microscopy techniques have emerged that allow optical imaging at unprecedented resolution beyond the diffraction limit. These techniques exploit photostabilizing buffers to enable photoswitching and/or the enhancement of fluorophore brightness and stability. A major drawback with the use of photostabilizing buffers, however, is that they cannot be used in live cell imaging. In this paper, we tested the performance of self-healing organic fluorophores, which undergo intramolecular photostabilization, in super-resolution microscopy examining both targeted (stimulated emission depletion (STED) microscopy) and stochastic readout (stochastic optical reconstruction microscopy (STORM)). The overall goal of the study was to identify dyes and conditions that lead to improved spatial and temporal resolution of both techniques without the need for mixtures of photostabilizing agents in the imaging buffer. As a result of previously shown superior performance, we identified an ATTO647N-photostabilizer conjugate as a potential candidate for STED microscopy. We have here characterized the photostability and resulting performance of this nitrophenylalanine (NPA) conjugate of ATTO647N on oligonucleotides in STED microscopy. We found that the superior photophysical performance resulted in optimal STED imaging and demonstrated that single-molecule fluorescent transients of individual fluorophores can be obtained with both the excitation- and STED-laser. In similar experiments, we also tested a nitrophenylacetic acid conjugate of STAR635P, another frequently used dye in STED microscopy, and present a characterization of its photophysical properties. Finally, we performed an analysis of the photoswitching kinetics of self-healing Cy5 dyes (containing trolox, cyclooctatetraene and NPA-based stabilizers) in the presence of Tris(2-carboxyethyl) phosphine and cysteamine, which are typically used in STORM microscopy. In line with previous work, we found that intramolecular photostabilization strongly influences

[5] These authors contributed equally to this publication.
[6] Author to whom any correspondence should be addressed.

Original content from this work may be used under the terms of the Creative Commons Attribution 3.0 licence. Any further distribution of this work must maintain attribution to the author(s) and the title of the work, journal citation and DOI.

photoswitching kinetics and requires careful attention when designing STORM-experiments. In summary, this contribution explores the possibilities and limitations of self-healing dyes in super-resolution microscopy of differing modalities.

Keywords: fluorescence microscopy, fluorescent dyes, super-resolution microscopy, STORM, STED

(Some figures may appear in colour only in the online journal)

1. Introduction

In recent years, pioneering developments in far-field fluorescence microscopy have revolutionized optical imaging. Commonly known as 'super-resolution microscopy' (or 'nanoscopy'), these techniques allow for visualization of biological structures beyond the physical diffraction-limited resolution of ~250 nm [1–8]. Super-resolution microscopy techniques all rely, to some extent, on ON/OFF-switching of fluorescence emission, i.e. photoswitching [9, 10]. The available techniques can be grouped into localization-based approaches using video-type fluorescence microscopy such as stochastic optical reconstruction microscopy (STORM) [1–3], photoactivated localization microscopy (PALM) [4], and point accumulation for imaging in nanoscale topography (PAINT) [5], or targeted-readout based approaches that are often realized in confocal setups, e.g. stimulated emission depletion (STED) [6], ground state depletion (GSD) [7], and reversible saturable optical linear fluorescence transitions (RESOLFT) [8].

As for any imaging approach that uses fluorescence as a 'molecular contrast' agent, the performance and properties of the fluorescent labels are of the utmost importance. It has become clear that a critical factor in obtaining a high spatial resolution is the physical size of the fluorescent label and its bio-linker [11, 12]. Furthermore, the signal generated by a fluorophore (the number of emitted photons per unit time) and its stability (the total time a fluorophore can emit photons) play an equally important role. In super-resolution techniques, another important property of the fluorophore is photoswitching [1–8], i.e. its ability to reversibly switch between an off- and on-state. In STORM, signal and photostability determine the image contrast, and allow for dynamic and time-lapse modalities. Photoswitching is required to overcome the diffraction-limited resolution [13–16]. Currently, a mixture of buffer additives (triplet-state quenchers, antioxidants and others) are often used to improve the photophysical properties of fluorescent labels while at the same time enabling photoswitching (thiol derivatives) [17, 18]. In the past few years, it became possible to use virtually any kind of synthetic organic fluorophore, fluorescent protein and even some semiconductor nanocrystals [19] for super-resolution microscopy.

More recently, intramolecular triplet-state quenching [20–22] of synthetic organic dyes ('self-healing' [23–25]) emerged as an alternative strategy to achieve high photostability [23, 26, 27]. The use of intramolecular triplet-state quenching overcomes some of the drawbacks of photostabilizers as buffer additives [23, 26–32]. For example, the addition of photostabilizers to the imaging buffer often creates conditions that are incompatible with biological requirements of living cells. Previous studies by our group demonstrated that self-healing dyes can be used for STED-type imaging of fixed mammalian cells [27], where a higher number of successive STED images could be acquired because of increased photostability [27]. The Blanchard lab has performed cellular imaging with self-healing dyes using various standard fluorescence microscopy techniques [23, 28].

While the improvement of fluorophore signal and count-rate are directly linked to photostability, the design of intrinsically blinking fluorophores (ON/OFF switching) remains a challenge and has only been realized successfully for a handful of examples [33, 34]. In this contribution, we explored the achievable spatial and temporal resolution of STED- and STORM-type microscopy techniques using self-healing dyes based on ATTO647N, STAR635P and Cy5. For this, we studied photostability, spatial resolution and brightness of single ATTO647N and STAR635P molecules in confocal and STED microscopy. We show that a single photostabilizer-ATTO647N derivative can provide MHz photon count rates, making the dye an ideal candidate for STED microscopy. Single molecule STED measurements of ATTO647N and NPA-ATTO647N revealed a significantly improved photostability of NPA-ATTO647N under STED imaging conditions. This allowed for multiple successive STED images of the same imaging area, even at elevated intensities of the STED laser. The use of NPA-ATTO647N resulted in a reduction of the point-spread-function down to ~30 nm and ~20 nm for NPA-STAR635P–values that are similar to the resolution achieved with solution-based additives (reducing oxidizing system (ROXS)) [12]. Additionally, for ATTO647N-photostabilizer derivatives it was possible to obtain fluorescent time traces of single dyes while illuminating with both the confocal excitation- and STED-laser. Finally, we explored the effects of intramolecular stabilizers (nitrophenylalanine (NPA), trolox (TX), cyclooctatetraene (COT)) on photoswitching kinetics of Cy5 for use in STORM. As a photoswitching agent we used reductive caging of fluorophores with tris(2-carboxyethyl) phosphine (TCEP) and the standardized condition in STORM, which is blinking of cyanine dyes with cysteamine (MEA). We found a strong influence of the stabilizers on the photoswitching kinetics of Cy5 that have to be taken into account whenever self-healing dyes are used in STORM-type imaging.

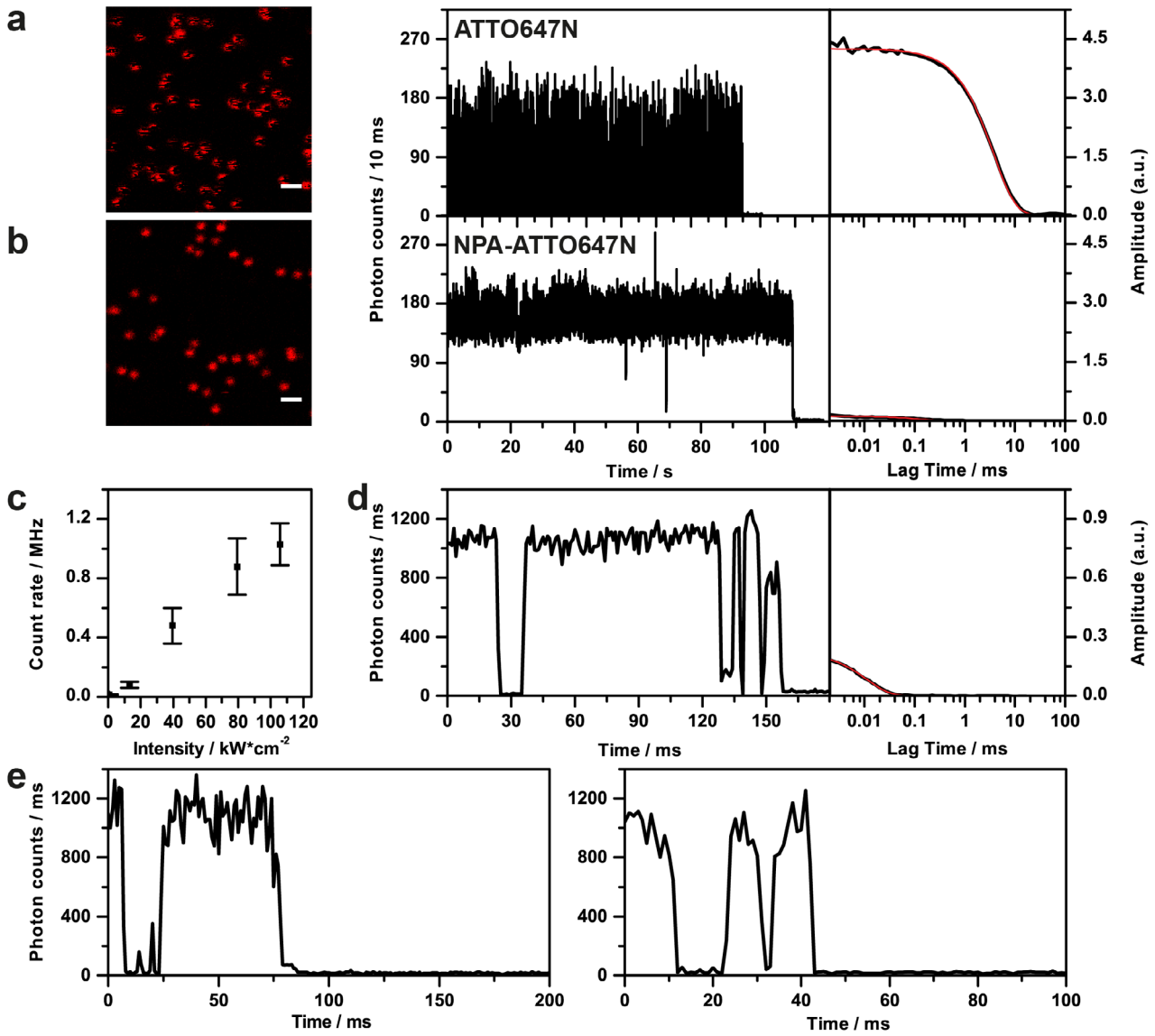

Figure 1. Photophysical characterization of NPA-ATTO647N with confocal microscopy. (a), (b) A representative confocal overview image (10×10 μm, 50 nm pixel size, 2 ms per pixel, scale bars are set to 1 μm) with spots from individual immobilized fluorophores (left), a fluorescence time trace (middle) and the corresponding autocorrelation decay (black) and fits (red) for ATTO647N (a) and NPA-ATTO647N (b). Image intensity scale from 5 to 100 counts, excitation intensity of ~0.66 kW cm^{-2} at 640 nm. (c) Intensity dependence of the fluorescent count rate of NPA-ATTO647N. (d) A confocal trace of NPA-ATTO647N at 100 kW cm^{-2} (excitation at 640 nm) with corresponding autocorrelation function (black) and fit (red). (e) Additional confocal traces of NPA-ATTO647N at 100 kW cm^{-2} (excitation at 640 nm).

2. Results

2.1. Photostabilizer-dye conjugates for increased photostability in STED microscopy

A key element for optical super-resolution is the control of the fluorescence emission signal (stable versus blinking) as well as photostability. Whereas STED microscopy requires stable and long lasting emission, photoswitching [6, 7, 10] is essential to PALM/STORM [1–4]. Here, we benchmarked the performance of ATTO647N, a widely-used carbopyronine fluorophore, and STAR635P, a phosphorylated rhodamine, on double-stranded DNA against their photostabilizer-dye conjugate. First, we investigated the photophysical behaviour of ATTO647N using single-molecule fluorescence microscopy. In the absence of oxygen, ATTO647N showed photobleaching times on the minute timescale, which was accompanied by frequent on/off blinking on the millisecond timescale (figure 1(a)). This blinking can be assigned to a triplet-related dark-state (off-state lifetime of 29 ± 5 ms) [27]. When bound to the photostabilizer NPA, the photophysical behaviour of ATTO647N changed and bright non-blinking molecules were observed (figure 1(b)). This was also seen in the autocorrelation curve where the triplet-related amplitude was strongly reduced (figures 1(a) versus (b)). As reported previously [27], the total number of detectable photons increased substantially (~4.5-fold; $N_{total} = 1.9 \pm 0.7 \cdot 10^5$ and $N_{total} = 8.6 \pm 0.4 \cdot 10^5$ for ATTO647N and NPA-ATTO647N, respectively). These observations suggest that NPA-ATT647N would be suitable dye for STED microscopy, where photostability, brightness

and signal-to-noise ratio (SNR) are important photophysical parameters.

In order to quantify the maximum brightness and obtainable signal-to-background (SNB) and SNR, we increased the excitation intensity from moderate levels (50 W cm^{-2}) up to 50–100 kW cm^{-2} (figure 1(c)). Under these conditions, a single NPA-ATTO647N fluorophore emitted with MHz rates (figure 1(c) and (d)). To the best of our knowledge, such high values have previously only been obtained with the help of plasmonic effects [35, 36] or for significantly shorter observation times [37] than used here (>50–100 ms). Count rates of 1000 counts ms^{-1} permit binning of the fluorescence signal with 50 μs resulting in SNR values of ~4–5. At intensities of 100 kW cm^{-2} an amplitude was found in the autocorrelation function with an off-state lifetime of < 10 μs (figure 2(d)). It is likely associated with an increasing population in the triplet-state and might reduce photon output and SNR at higher excitation intensities.

Next, we tested whether NPA-ATTO647N exhibited enhanced photostability under STED imaging conditions. Figure 2 shows alternating confocal and STED images of ATTO647N and NPA-ATTO647N under deoxygenated conditions. In the sequence of images, the confocal image was taken first. Subsequently, an image of the same area was recorded with the STED beam overlaid to the confocal excitation beam. Finally, a second confocal image was recorded and compared to the first confocal image. In figures 2(a) and (b), an analysis method was adapted from Kasper *et al* [12]. From the composite image (confocal 1 + 2), it can be seen that a significant population of the ATTO647N molecules were photobleached after one scan of the field of view with the STED laser. In contrast, the majority of NPA-ATTO647N molecules survived even a second cycle of confocal/STED imaging (figures 2(b) and (c), inset), as evidenced by the number of yellow spots in the confocal 1 + 2 image (figures 2(a) and (b)). These results suggest that intramolecular photostabilization remains effective not only for fluorescent labels in fixed cells [27] but also for single-molecules under STED imaging conditions and high excitation power.

For a quantitative analysis, the same series of alternating confocal and STED images was repeated at different powers of the STED beam (figure 2(c)). At low power, it can be seen that already ~25%–45% of individual ATTO647N fluorophores were photobleached after or during the acquisition of one STED image, whereas for NPA-ATTO647N, almost all molecules were still fluorescent after STED imaging. Upon increasing the laser power of the STED beam, i.e. up to 60 mW, still >60% of the NPA-ATTO647N molecules did not photobleach after one STED-image. Further increasing the STED laser power photobleached almost all (>90%) of the ATTO647N fluorophores, whereas >25% of the NPA-ATTO647N molecules were still fluorescent. At 100 mW of STED power, ~6% of the single NPA-ATTO647N fluorophores survived the STED image acquisition. In contrast, <2% of the ATTO647N fluorophores were detected. We have assumed here that in general, a higher power of the STED laser results in an increased resolution [6, 10, 12].

In a next step, an intermediate STED laser intensity of 50 mW was used to acquire multiple subsequent confocal and STED images. Under these conditions, a significant fraction of fluorophores are not photobleached after one STED-image was acquired, but the spatial resolution is close to the experimentally observed optimum of ~30 nm PSF width. In figure 2(c) (inset) the remaining number of fluorophores after one and two confocal-STED-confocal imaging cycles is shown. Once again, the difference between NPA-ATTO647N and its parent fluorophore is substantial, with ~60% versus ~20% survival, respectively. This imaging mode with photostabilizer-dye conjugate allows multiple successive STED images of the same area to be taken with a drastically reduced loss of fluorescent signal (increased photostability), potentially enabling time-lapse STED imaging.

Next, we studied the XY-resolution as a function of the intensity of the STED laser. In the confocal image, a Gaussian of the microscope's point-spread function resulted in a FWHM of 225 ± 26 nm for NPA-ATTO647N (figure 3(a)).

Overlaying the confocal excitation beam with the STED beam resulted in an increase in the resolution, which was reflected in a decrease in the FWHM of the point-spread-function, PSF (figure 3(a)). The optimal resolution was achieved for powers >50 mW and a PSF of 29 ± 5.6 nm (for STED conditions the point spread functions were fitted using a 2D Lorentzian function [38–40], figure 3(a)), which is consistent with values found in literature [12]. For each STED power, >20 molecules were analysed using a 2D Lorentzian fit. At high intensities of the STED laser >40 mW, the FWHM of NPA-ATTO647N was slightly lower compared to ATTO647N (figure 3(a)). Additionally, the variation of the FWHM at a specific STED laser intensity was higher for ATTO647N without any photostabilizer. From the images in figures 3(b) and (c), it is clear that ATTO647N (figure 3(b)) showed multiple pixels with no detectable fluorescence. This is caused by the blinking characteristics of ATTO647N (see also fluorescence in figure 1(a)) during raster scanning and image acquisition. As a result, it is likely that during the acquisition of an image, the fluorophore does not emit photons during the scan in between different positions, which results in dark pixels. This observed subtle difference in resolution might, however, have a real-world equivalent in STED imaging, because the signal from one emitter is not continuous. The observed saturation of the resolution decrease at >50 mW can be attributed to limitations of the experimental setup and the length of the dsDNA construct used here, as has been reported elsewhere [12].

STED microscopy has become a useful tool for high-resolution imaging and our previously published studies with KK114/STAR-RED [27] and here ATTO647N suggest the potential of photostabilizer-dye conjugates for time-lapse STED-imaging in (fixed) cells. To probe the available photon-output from individual molecules under STED conditions, something that is potentially useful for dynamic studies such as STED-FCS [41] of densely-labelled environments, ATTO647N and NPA-ATTO647N were compared in a dynamic imaging mode (figure 4).

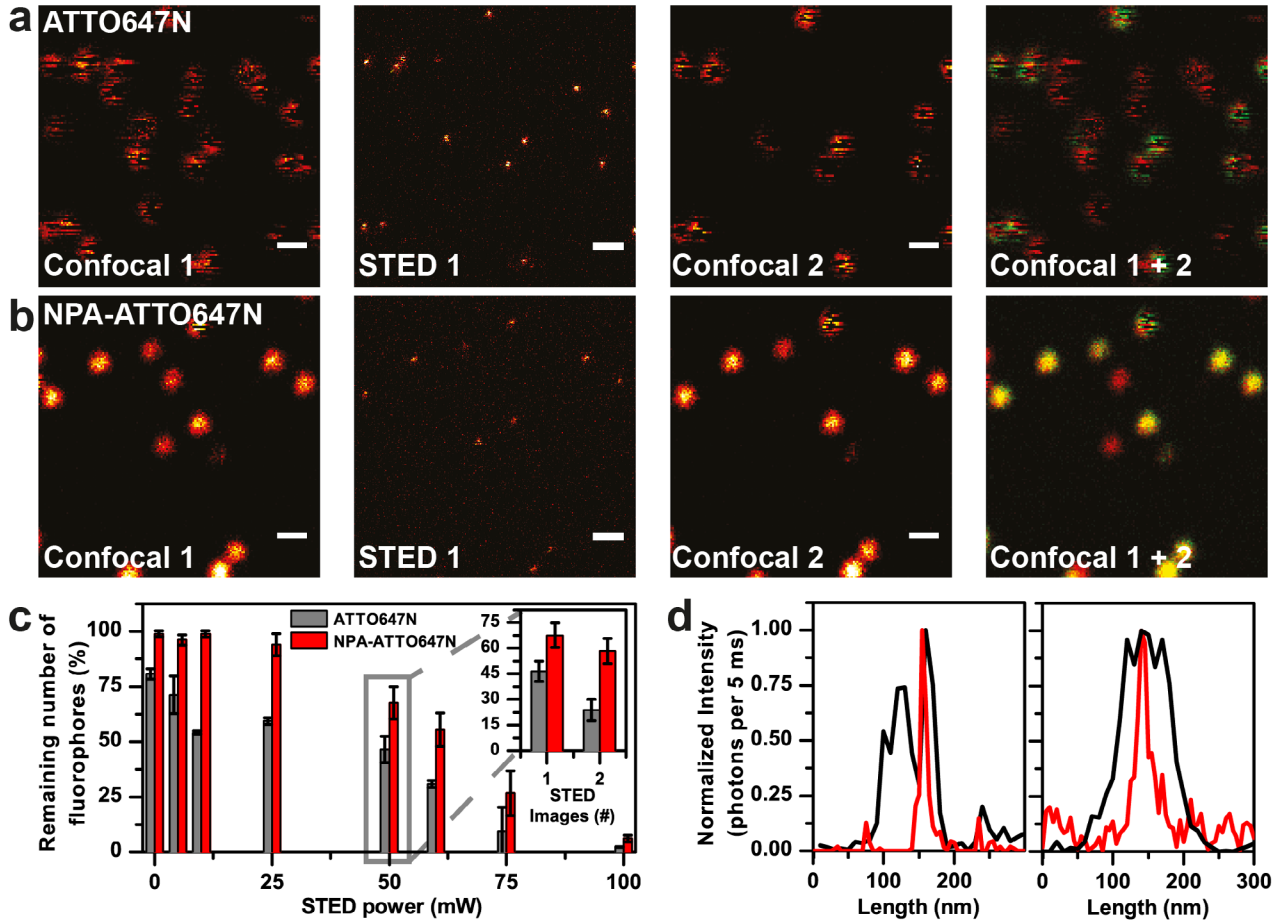

Figure 2. STED microscopy of individual ATTO647N derivatives. Alternating confocal, STED and confocal images of single (a) ATTO647N and (b) NPA-ATTO647N labelled oligonucleotides. Confocal 1 + 2 is a composite image of the first and second confocal image to visualize the number of remaining single molecules after a single STED image acquisition. (c) Quantitative analysis of the remaining number of fluorophores in a confocal image after acquiring a STED image at different STED laser powers for ATTO647N and NPA-ATTO647N. At 50 mW STED laser power, the remaining number of fluorophores in a confocal image was analysed after acquiring one or two STED images (insert). (d) Line profiles of a single ATTO67N (left) and NPA-ATTO647N (right) molecule in confocal (black) and corresponding STED (red) image. The confocal images were recorded at 640 nm excitation with 3.4 kW cm^{-2}. The STED images were recorded with 640 nm excitation at 3.4 kW cm^{-2} complemented with a STED beam at 765 nm with 50 mW at the sample ((a) and (b)). Scale bars are set to 500 nm. All data was recorded with a sample in aqueous PBS buffer at pH 7.4 in the absence of oxygen.

Next to STED images, a representative single molecule fluorescence time trace is shown under conditions where the STED beam is activated. For ATTO647N, no fluorescence signal was observed under these conditions (figure 4(a)). In contrast, with NPA-ATTO647N, fluorescence signals were observed that persisted for many seconds (figures 4(b) or (c)). These results demonstrate that intramolecular photostabilization of organic fluorophores effectively enhances the photophysical properties of fluorophores for STED-type super-resolution microscopy and enable dynamic imaging modes. We believe that the use of self-healing dyes for STED microscopy can be extremely beneficial especially in combination with recent developments like protected STED [42].

Another popular fluorophore for STED imaging is STAR635P, a phosphorylated rhodamine derivative developed by the Hell-lab [43]. The dye was tailored for high water-solubility and optimal performance in STED. To complement our studies of ATTO647N, we here provide a qualitative comparison of data from both dyes (figures 5 and 6). To our knowledge, the photophysics of STAR635P at the single-dye level has not yet been characterised. To allow comparison of the data in figures 5 and 6 to other previously published fluorophores, we used the same 40-mer double-stranded DNA scaffold as a handle for immobilization.

Using a confocal scanning microscope, we characterized STAR635P and STAR635P-NPAA terminally-attached to dsDNA. The parent fluorophore STAR635P (figure 5(a)) showed high brightness in oxygenated PBS buffer with count rates of ~100 kHz at 2 kW cm^{-2} excitation intensity. Note that this was three-fold higher excitation power than used to collect the data in figure 1 for ATTO647N (which was excited with only 0.66 kW cm^{-2}). In light of the difference in conditions used, STAR635P still showed higher brightness compared to ATTO647N and also shorter off-periods while blinking when oxygen is present (compare figure 5(a) to traces of ATTO647N in PBS from [27] where the off-periods typically last a few seconds). With ROXS conditions, no blinking was observed for STAR635P and the fluorophore emitted stably and at a high count-rate, although with substantially shorter photobleaching lifetimes when compared

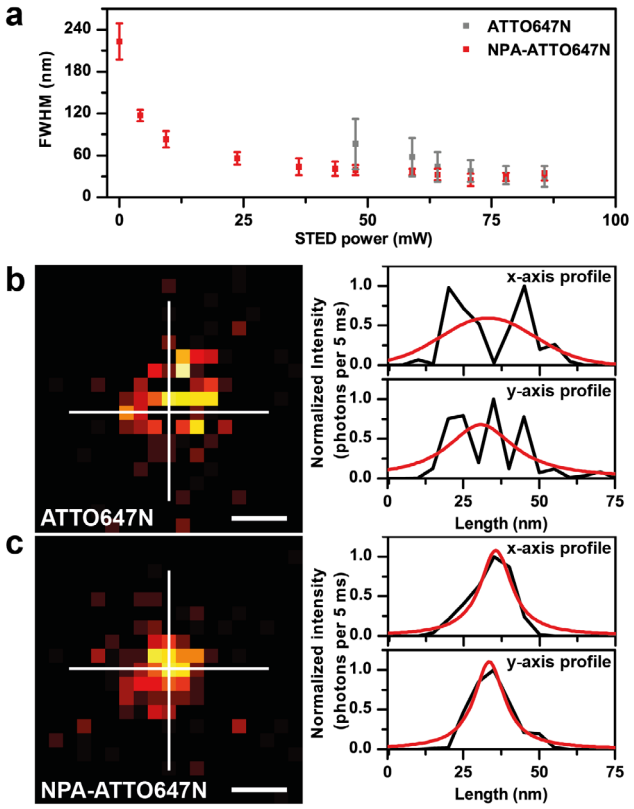

Figure 3. (a) Quantitative analysis of the PSF of ATTO647N (full width at half maximum, FWHM) at different STED laser powers. The STED images were recorded with 640 nm excitation at 10 kW cm^{-2} complemented with a STED beam at 765 nm with varying powers at the sample. (b), (c) STED images of single ATTO647N (b) and NPA-ATTO647N labelled oligonucleotides (640 nm excitation at 3.4 kW cm^{-2} complemented with a STED beam at 765 nm with 50 mW at the sample, scale bars are set to 20 nm with 5 nm/pixel). All data was recorded with a sample in aqueous PBS buffer at pH 7.4 in the absence of oxygen.

to ATTO647N. Proximity of NPAA to STAR635P (figures 5(c) or (d)) reduced the brightness to about 1/3 of the original signal. Since the fluorescence lifetimes of the dye are only altered by ∼20% in different environments and upon conjugation to NPAA (STAR635P, PBS: 3.8 ± 0.1 ns; STAR635P, ROXS $-O_2$: 3.8 ± 0.1 ns; STAR635P-NPAA, PBS: 3.2 ± 0.1 ns; STAR635P-NPAA, $-O_2$: 3.1 ± 0.1 ns; errors are standard deviations from ~15 molecules) we interpret this as combined dynamic and static fluorescence quenching. Dynamic singlet quenching alone could not account for the large reduction of the fluorescence signal. The overall trends and photophysical character were, however, not changed upon the addition of NPAA since STAR635P-NPAA alone showed shorter off-periods when blinking in the presence of oxygen (figure 5(c)). In the absence of oxygen, the blinking was suppressed (figure 5(d)). STAR635P-NPAA showed short on-periods when blinking in several traces (see figure 5(d), middle trace), which indicates long interactions of the stabilizer with STAR635P that are removed shortly. In various cases, we also observed reduction of the signal to a dim-state before final photobleaching when NPAA was present (figure 5(d)).

Interestingly, these characteristics (figure 5) translated into excellent behaviour of the dye under STED conditions (figure 6). This was unexpected because STAR635P-NPAA showed compareble brightness but modest photostability, and an overall photon-output comparable to ATTO647N. In line with the popularity of STAR635P for STED in various biological settings, the average PSF of STAR635P-NPAA was 17 ± 3 nm, which was nearly 2-fold better than the values obtained for ATTO647N. STAR635P-NPAA increased the resolution in the STED mode more than 13-fold from 226 nm to 17 nm, a value approaching the length of the dsDNA 40-mer. Strikingly, this value is better than the one reported for ATTO647N with ROXS [12], and suggests the STAR635P fluorophore can be used as a self-healing dye for STED microscope despite the singlet-quenching and resulting signal reduction. It remains to be answered, quantitatively, how much improvement can be for STAR635P in STED microscopy via the self-healing process.

2.2. Photostabilizer-dye conjugates for localization-based STORM microscopy

Thus far, we and others were able to demonstrate that self-healing dyes based on distinct fluorophore-scaffolds (cyanines, rhodamines, carbopyronines, fluoresceins) [19, 27] have an increased photostability compared to their non-stabilized counterparts [27]. This turned out to be particularly useful for STED-type microscopy (see the previous section of this paper) where the number of possible excitation cycles limits the attainable resolution [10]. For STORM/PALM type super-resolution, however, additional functionality is required. In particular the emission pattern of one fluorophore needs to display photoswitching kinetics with a characteristic low ON/OFF ratio [44]. This allows a situation in which the majority of fluorophores molecules are inactive to separate individual fluorescent labels in a structure via single-molecule localization [1–5, 10, 45].

Related to this requirement, our group recently reported the effects of intramolecular photostabilizers on the action of solution-based additives such as TX, COT, TCEP and cysteamine (MEA) [46]. In that paper, we evaluated the competition between inter- and intramolecular triplet-state quenching processes and showed that they were neither additive nor synergistic. Our findings revealed that intramolecular processes dominate the photophysical properties of different organic fluorophores for combinations of covalently linked and solution-based photostabilizers, and importantly also photoswitching agents used for STORM. In that study [46], we verified the function of intramolecular photostabilizers to protect fluorophores from reversible photoswitching by solution additives. Additionally, evidence was provided that the biochemical environment and in particular the proximity of aromatic amino-acids such as tryptophan, significantly reduced the photostabilization efficiency of commonly used buffer cocktails [46].

Here, we detail the effects of the intramolecular photostabilizers TX, NPA and COT for Cy5 photoswitching kinetics and photon-yields, i.e. parameters relevant for STORM-type microscopy. We used an established approach where single-molecule TIRF-microscopy provides information on

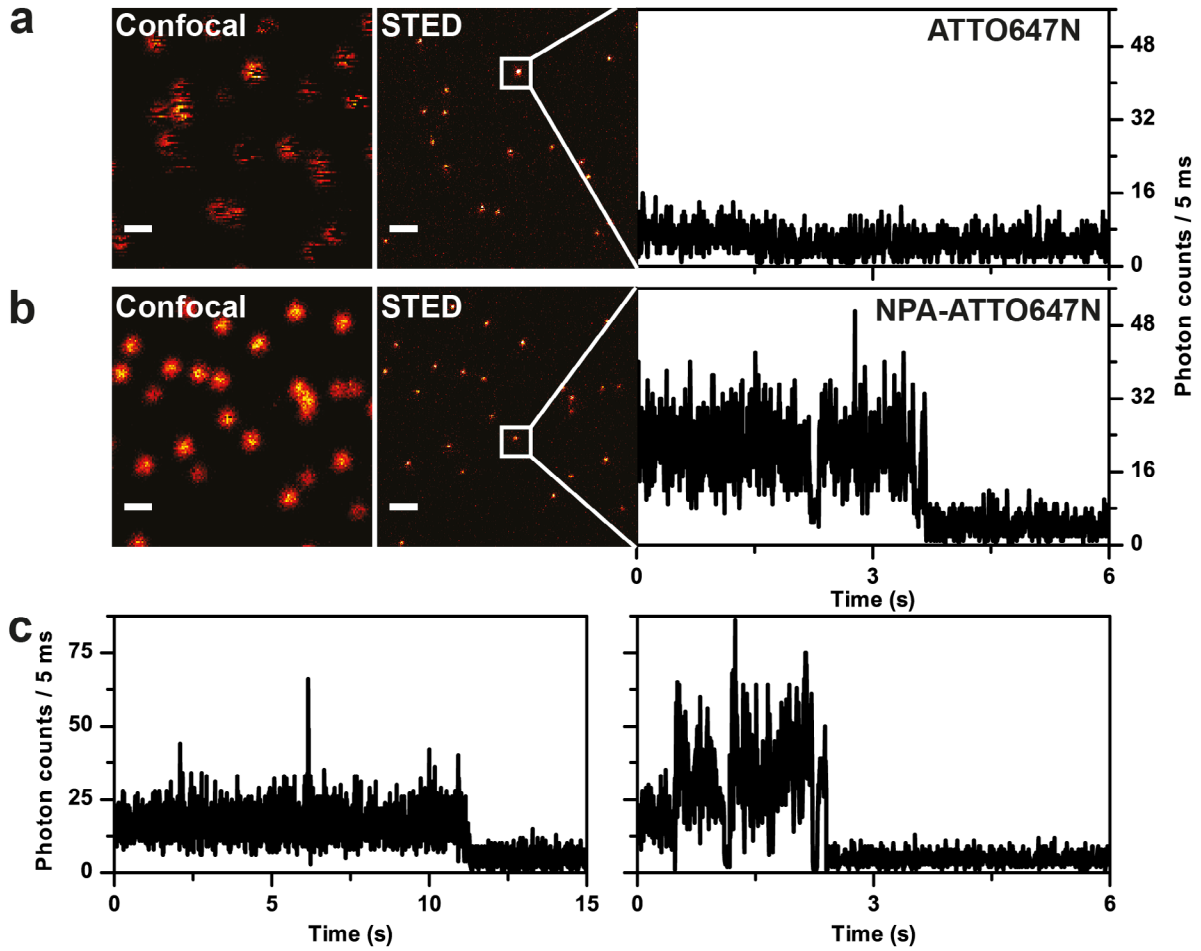

Figure 4. Single molecule fluorescence time traces under STED conditions for (a) ATTO647N and (b) NPA-ATTO647N. Each panel consists of a confocal image, STED image and single molecule fluorescence time trace recorded under STED conditions. (c) Additional single molecule fluorescence time trace of NPA-ATTO647N recorded under STED conditions. The fluorescent time traces correspond to the fluorescent spots from the same STED image in (b) but their location is not indicated. The confocal images were recorded at 640 nm excitation and 3.4 kW cm^{-2}. The STED images and single molecule fluorescence traces were recorded with 640 nm excitation at 3.4 kW cm^{-2} complemented with a STED beam at 765 nm with 50 mW at the sample. Scale bars are set to 500 nm. All data was recorded with a sample in aqueous PBS buffer at pH 7.4 in the absence of oxygen.

photobleaching lifetime, count-rate, signal-to-noise ratio and total photon-count of individual fluorophores tethered to dsDNA on a microscope coverslide (figure 7(a)) [26, 46]. It has to be stressed, that the time-point where signal-loss occurs (see figure 7(a), where the signal abruptly decreases to background level) might reflect either irreversible photobleaching or UV-reversible off-switching. In line with our previous work, we refer to this as 'apparent photobleaching lifetime' [46], which reflects both pathways for fluorescence deactivation.

Since our main interest was the comparison of results in the presence and absence of TCEP in the imaging buffer (figure 7(a)), we provide normalized values of all parameters (figures 7(b) or (c)). As shown previously [46], already lower concentrations TCEP can have a major influence on the photophysical properties of different organic fluorophores (figures 7(b) or (c)). Interestingly, carbopyronines were not influenced in their photophysical properties when TCEP was added to the solution (figure 7(b)), which renders them unsuitable for STORM-microscopy in combination with TCEP. As expected from previous work of the Zhuang-lab [47], Cy5 undergoes rapid photoswitching once TCEP is present. Unexpectedly, already 200 μM was sufficient to switch Cy5 efficiently off, while SNR and count-rate were unaltered (figure 7(c)) [46]. Upon addition of TCEP, the fluorescence of Cy5 was quenched due to a 1,4-addition of the phosphine to the polymethine bridge of Cy5 [48]. It can indeed be seen from figures 7(b), (c) and 8(b), (c) that the presence of TCEP results in faster signal loss of Cy5 molecules.

In the absence of TCEP, the decay was a result of photobleaching whereas in the presence of TCEP, the ~10× faster decay was attributed to photoswitching by TCEP (figure 7(c)). Subsequently, illumination with UV dissociates the covalent adduct to restore (and activates) 51% ± 8% of the Cy5 fluorophores (see figures 8(b) and (c) and Vaughan *et al* [48]), which we also investigated by TIRF microscopy. We determined the percentage of activation using the number of fluorophores in the first frames 1–10 at the start of each experiment (to account for blinking molecules, figure 8(a)). Subsequently, the remaining number of spots after apparent photobleaching (frames $n - 10$ to n) and the number of molecules that were activated over the course of illuminating the surface area

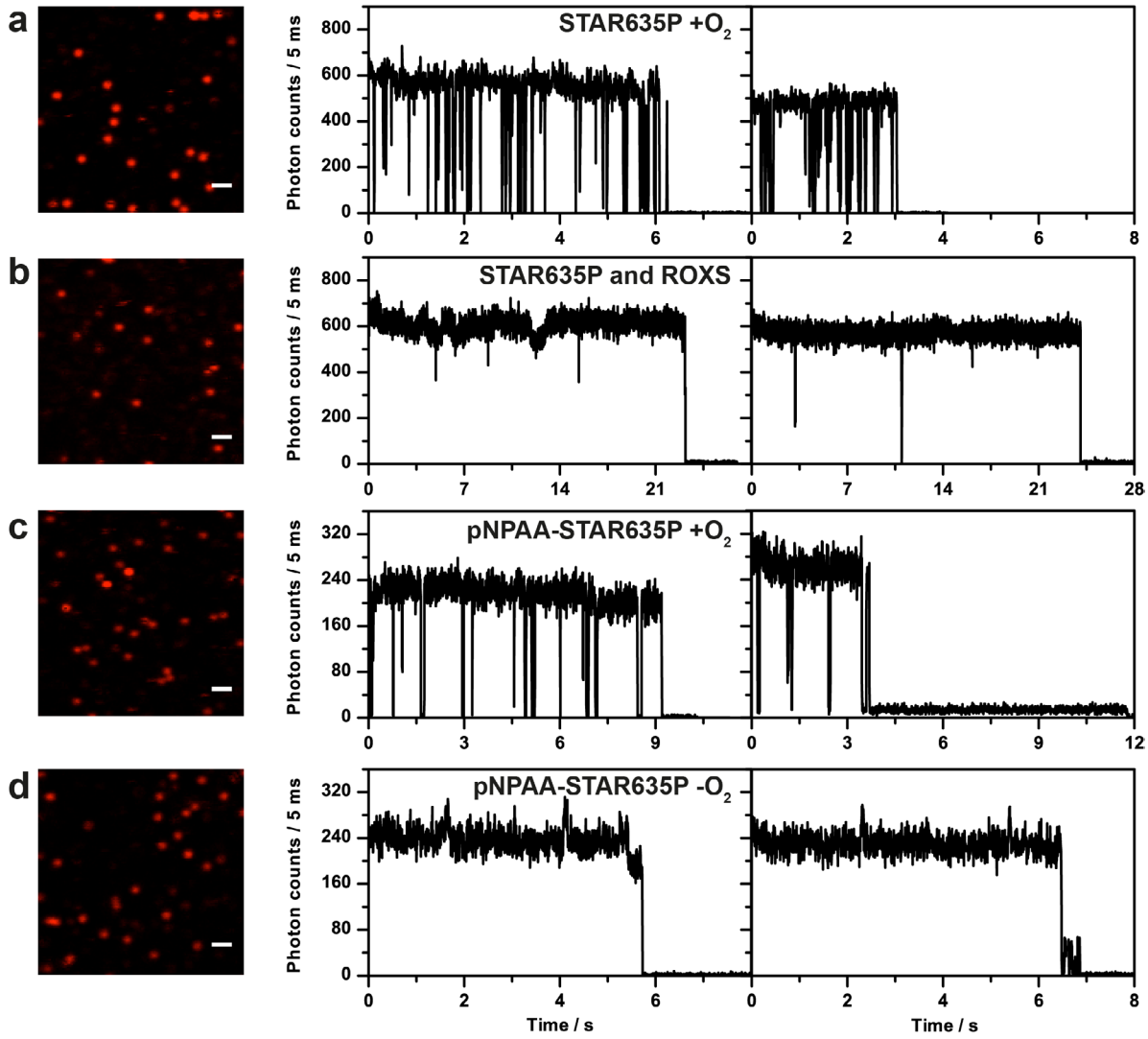

Figure 5. Photophysical characterization of STAR635P and its proximal conjugate with NPAA on dsDNA by confocal microscopy. A representative confocal overview image (10 × 10 μm, 50 nm pixel size, 2 ms per pixel, scale bars are set to 1 μm) with spots from individual immobilized fluorophores (left), and fluorescence time traces (right) for (a) STAR635P, (b) STAR635P with ROXS, (c) STAR635P-NPAA and (d) STAR635P-NPAA in deoxygenated conditions. Excitation power was 2 kW cm^{-2}, which is three-fold higher than for ATTO647N in figure 1.

with UV (405 nm, frames 1 to m) were determined. Here, the number of frames used depends on the photobleaching time of the fluorophore (figure 8(a)).

Results in figure 8(c) show that there is little activation of Cy5 in the absence of TCEP. We consequently sought to determine the effect of additional buffer additives COT and TX, in addition to TCEP, on blinking and the photon yield (figure 8(c)) [17]. The addition of COT to Cy5 in the absence of TCEP resulted in an increased signal duration (figure 8(c), grey bars). The presence of TCEP together with COT quenched Cy5 (with an observed photobleaching lifetime that is ~3× faster) with 25% ± 5% of fluorophore that was activated upon illumination with UV. In contrast, the combination of TX and TCEP did not result in fast off-switching and a high UV-reactivation yield of Cy5. Instead it was observed that photobleaching occurs substantially faster in the absence of TCEP with TX. TCEP thus seems to be required for photostabilization using TX. These results also support the observed complexity of stabilization mechanisms for TX via oxidation [49] and geminate recombination pathways [50]. We hypothesize that there is a competition between TCEP as photoswitching agent and as photostabilizer when used in combination with TX. In this specific combination, the photostabilization pathway seems more dominant, which is also reflected in the activation percentage showing no significant activation for TCEP and TX (figure 8(c)).

In a second step, TCEP quenching was used in combination with photostabilizer-Cy5 derivatives (NPA-Cy5, COT-Cy5 and TX-Cy5). As can be seen in figure 8(c), there was no significant difference between the photobleaching lifetimes in the absence or presence of TCEP for all three constructs. However, the activation percentages do show that activation occurs only in the presence of TCEP. For NPA-Cy5, the activation in the presence of TCEP was negligible, whereas it was significant for COT-Cy5 and TX-Cy5 (14% ± 4% and 19% ± 4%, respectively).

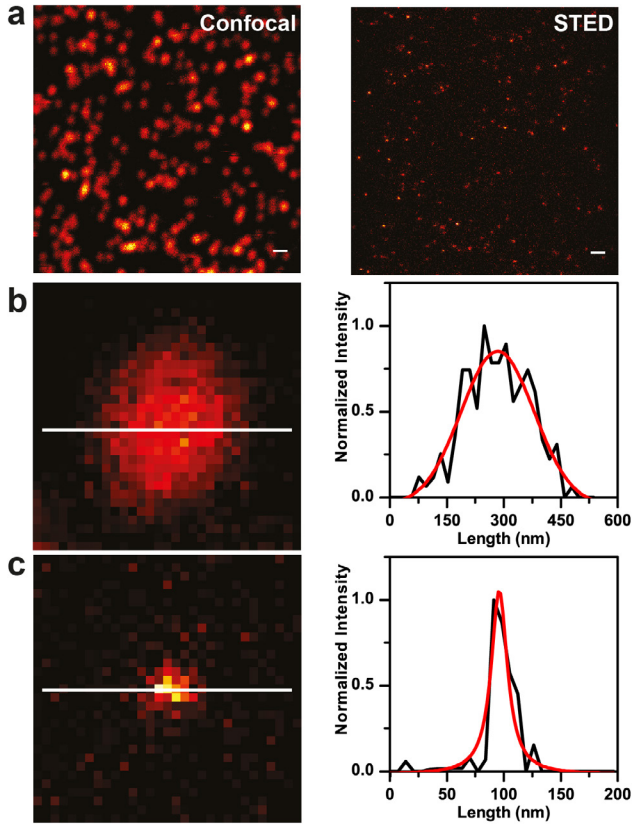

Figure 6. STAR635P-NPAA and STED. (a) A representative confocal overview image (left) and a STED overview image (right) of same area with spots from individual immobilized STAR635P-NPAA fluorophores (9×9 μm, 100 μs dwell-time per pixel, scale bars are all set to 500 nm. Here the excitation power used was 30 μW at 637 nm; for the STED image the excitation light was overlaid with a STED beam at an intensity of 200 mW). (b) STED image of a single STAR635P-NPAA fluorophore (right) and a plot-profile (black line) and corresponding Gaussian fit (red line, FWHM $= 226 \pm 14$ nm) of the cross-section (right). (c) STED image of a single STAR635P-NPAA fluorophore (right) and a plot-profile (black line) and corresponding Lorentzian fit (red line, FWHM $= 17 \pm 3$ nm) of the cross-section (right).

This apparent contradiction between the unaltered photobleaching times and the activation for COT/TX-Cy5 might be explained by the use of a low concentration of TCEP. At 200 μM TCEP, there is a competition between photobleaching of the photostabilizer-Cy5 conjugates and photoswitching via TCEP. As we could show before, TCEP has an equilibrium contribution of photoswitching but additionally appears to be switched-off through a photo-induced step involving the triplet state of the fluorophore [46]. In the photostabilizer-Cy5 derivatives however, TCEP-based triplet-quenching (resulting in reversible off-switching) and bleaching cancel each other, a fact that results in unaltered photobleaching lifetimes in the presence and absence of TCEP. Consequently, UV-induced on-switching can only be observed with TCEP.

It is therefore hypothesized that when an increased concentration of TCEP was used, the apparent photoswitching pathway via TCEP would become more prominent and results in an increased activation percentage upon illumination with UV. To test this hypothesis, the concentration of TCEP was increased to 25 mM. In figure 8(c), it is shown that an increased TCEP concentrations results in a reduced photobleaching lifetime of Cy5-COT (i.e. faster off-switching). Upon applying UV-illumination, the number of activated Cy5-COT fluorophores was indeed (figure 8(c)) increased compared to 200 μM TCEP. This can be interpreted as a higher concentration of TCEP resulting in more photoswitching of Cy5-COT. While this comparison is not sufficient to reveal the full concentration dependence for TCEP, it provides support for its mode of action and the hypothesis of increased apparent photoswitching at higher TCEP concentrations. A similar mechanism might also apply for conditions of Cy5 in the presence of 2 mM COT in solution, where COT efficiently quenches the fluorophores triplet. Looking at the apparent on-times of the different fluorophores upon simultaneous excitation and UV-illumination, it was observed that the on-times increased upon applying photostabilization. Therefore, the photon yield per on-period increased. It can be seen that with COT as a photostabilizer in solution, the highest on-times were observed. Nevertheless, for constructs with intramolecular photostabilizer, the on-times increased significantly compared to Cy5. As a result, the number of photons coming from a single fluorophore, which, as explained previously, is needed to make STORM/PALM techniques useful, increased per on-cycle. The presented trends might allow the establishment of guidelines to enable the prediction of the effect of intramolecular photostabilizers on photoswitching kinetics for common buffer additives.

We also tested cysteamine (MEA) as a photoswitching agent for Cy5, in combination with 2 mM COT in solution and self-healing Cy5-COT. Figure 9 shows that with 5 mM MEA, the apparent photobleaching lifetime was reduced compared to the use of TCEP. This was also true when used for Cy5 in combination with COT as a photostabilizing agent in the imaging buffer. However, looking at the activation percentages upon applying UV, it can be seen that only for Cy5 in the absence of COT, also the activation percentage has increased further when using MEA. For all other conditions the activation efficiency of MEA is lower compared to TCEP.

Finally, we studied the on-times after photoactivation for molecules/conditions with reactivation efficiencies $> 15\%$. Interestingly, the on-time for the condition of Cy5 with COT in solution is doubled when cysteamine is present. The on-times for Cy5 and Cy5-COT were reduced when cysteamine was added. This was a result of a decreased photon-yield obtained from a single molecule. Consequently, it is less useful for STORM/PALM techniques.

3. Discussion and conclusions

Our results show that intramolecular photostabilization of organic fluorophores effectively enhances their photophysical properties such as brightness and photostability, but also alters their photoswitching kinetics. Photostabilizer-dye conjugates show an increased photostability and brightness, which are important parameters for *in vivo* and *in vitro* STED microscopy applications. Upon covalent binding of a nitrophenyl

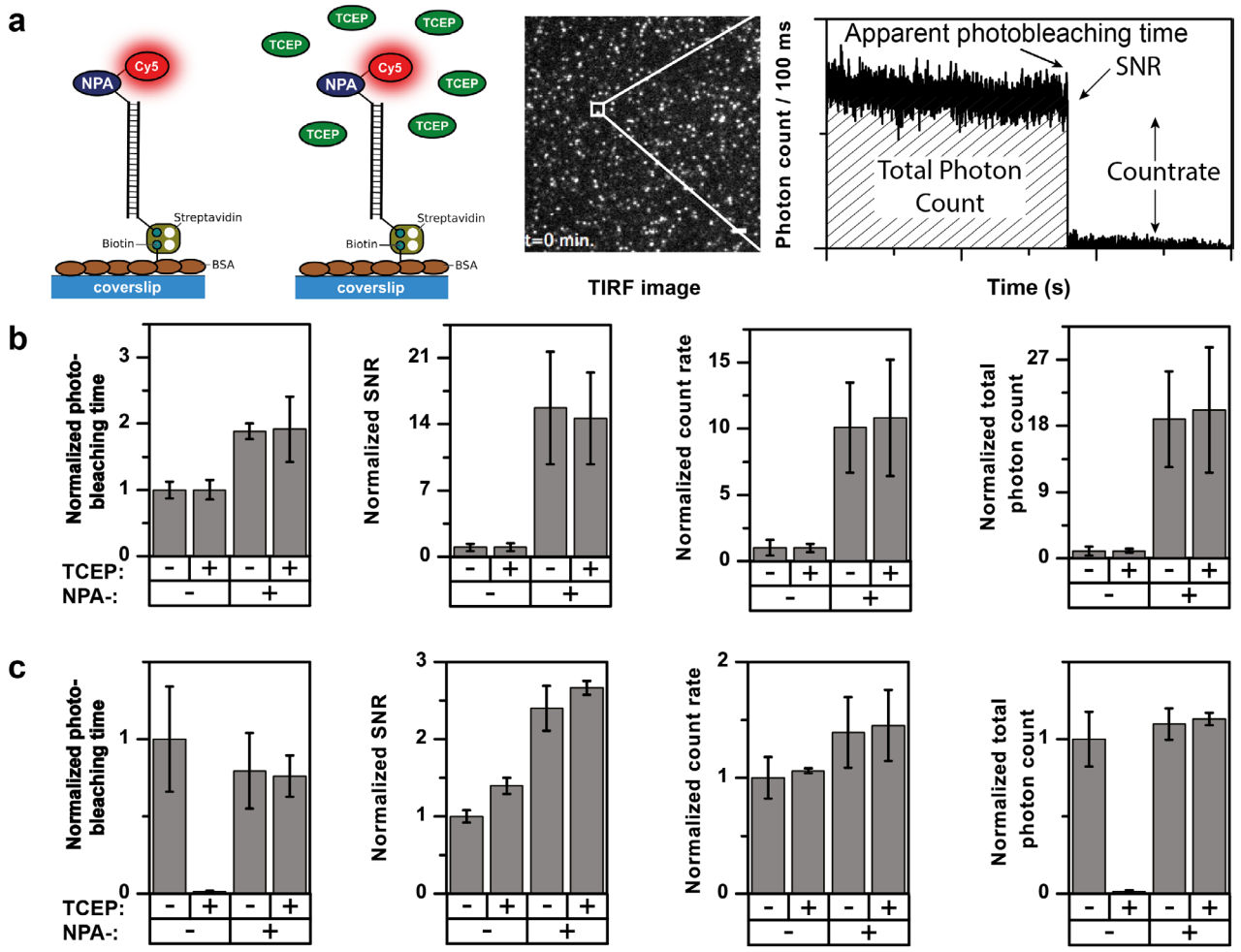

Figure 7. TIRF imaging of Cy5 and ATTO647N derivatives to determine photostability in the presence and absence of TCEP. (a) Schematic of the experimental setup of dsDNA-NPA-dye constructs immobilized via BSA-biotinylated coverslips and a typical fluorescent time-trace obtained in TIRF microscopy. Photophysical characterization of (b) ATTO647N and NPA-ATTO647 (c) Cy5 and NPA-Cy5 in the absence or presence of 200 μM TCEP. All imaging was done under deoxygenated conditions with 400 W cm^{-2} excitation at 637 nm. Error bars show standard deviation of repeats on three different experimental replicates. Data in the figure partially adapted from Smit *et al* [46].

moiety to ATTO647N, single molecule count rates of up to MHz were obtained. It was found that intramolecular photostabilization significantly improves the photostability of ATTO647N when excited with both the confocal excitation and STED beam, thereby increasing the number of possible subsequent STED images that can be acquired. Additionally, on average lower STED laser intensities were needed to obtain the maximum resolution ~30 nm with NPA-ATTO647N when compared to ATTO647N, thereby reducing the probability of photobleaching of the fluorophores and phototoxicity to the sample. The improvement of photophysical parameters by intramolecular photostabilization paves the way for dynamic STED imaging without the need for adding (potentially toxic) chemical compounds [12]. Our results also show that the phosphorylated rhodamine STAR635P, often used for STED, exhibits prominent singlet-quenching and signal reduction in proximity to NPAA. While this is an unwanted effect it did not compromise the excellent properties of STAR635P in STED and allowed a resolution of ~20 nm for single fluorophores on oligonucleotide structures.

We could further show how intramolecular photostabilizers affect the photoswitching kinetics of TCEP and MEA in combination with Cy5. Both TCEP and MEA were found to reversibly switch-off Cy5 and its self-healing photostabilizer-conjugates, allowing reactivation upon UV illumination. The photostabilizer, had, however, a large effect on the photoswitching kinetics. By adjusting the TCEP concentration, both the reactivation percentage and on-times of photostabilized conjugates could be optimized allowing their application in STORM-type super-resolution imaging. When using MEA as a photoswitching agent, we found a reduced apparent photobleaching lifetime, which was not translated into a corresponding increase in reactivation percentage. The reduction in photobleaching time can therefore not be attributed to the formation of a MEA-induced reversible dark state. This discrepancy was also observed when COT is present in both inter- and intramolecular photostabilization, which suggests that either MEA interferes with reactive intermediates in the mechanism of photostabilization. Alternatively, it seems possible that in the presence of photostabilization

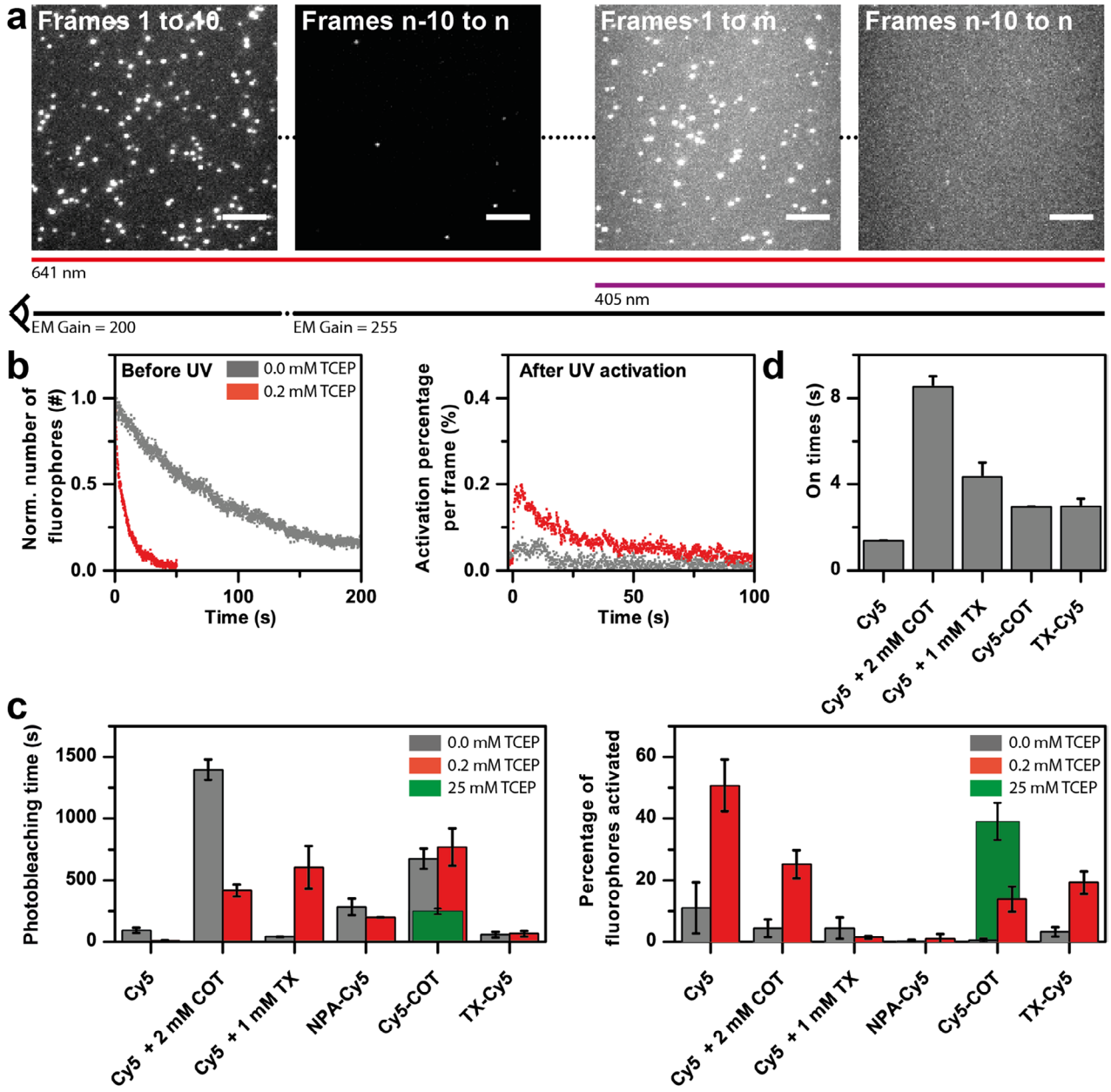

Figure 8. Photoswitching and UV-activation of Cy5 derivatives with TCEP. (a) TIRF images at different time points and under different illumination conditions. (b) Decay curve (left) and activation curves (right) of the number of Cy5 fluorophores without (grey) and with (red) TCEP. (c) Histograms of the photobleaching time (left) and activation percentages (right) of different Cy5 conjugates with (red) and without TCEP (red, green). (d) On-times (ms) of the different Cy5 conjugates. The on-times are extracted from the fluorescent time traces. Error bars are SD except for 25 mM TCEP, where SEM is shown. Data in the figure was partially adapted from Smit *et al* [46].

a different dark state is formed which is less susceptible to UV-induced photoactivation. The longest on-times were observed when using MEA with COT as a photostabilizer in solution. This suggests that this combination allows collecting the most photons per activation. Therefore, further investigation should be aimed towards identifying potential interactions between COT photostabilization and thiol-based photoswitching agents, which can provide guidance in optimizing the reactivation efficiency when COT is employed as a photostabilizer.

In conclusion, our findings have various implications for the use of self-healing dyes for STED and STORM, where both optimal photon-yield and photoswitching are required. Previously, we showed that the effects of photostabilizers on photoswitching kinetics might explain why the same dye has completely different photoswitching in different biochemical surroundings, e.g. antibody versus DNA or protein [46]. This emphasizes that also the environment has to be taken into account whenever quantitative values for photobleaching or photoswitching kinetics are reported [46]. Furthermore, we found that such effects were most pronounced for Cy5 dyes but almost negligible for Alexa555 and ATTO647N.

From this previous study [46] and results reported here, the emerging picture is that their use is straight forward whenever photostability is the key criterion for super-resolution imaging. This renders them ideal candidates for confocal

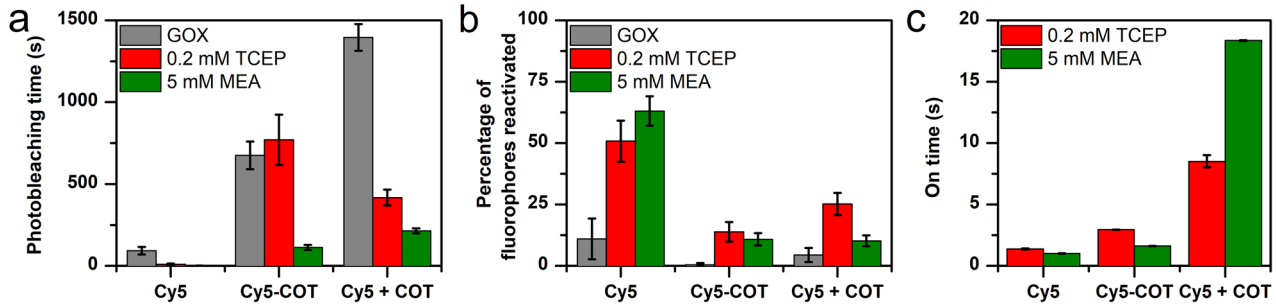

Figure 9. Comparison of Cy5 with inter- and intramolecular photostabilizer COT and with reversible off-switching by 0.2 mM TCEP and 5 mM MEA. (a) Photobleaching lifetime (b) percentage of fluorophore recovered by 405 nm excitation. (c) Mean on-state lifetime of reactivated fluorescent transients in case of reactivation. Error bars are standard deviations of independent repeats of different days (a) and (b) or SEM (c). Data in the figure partially adapted from Smit *et al* [46].

microscopy techniques, STED, RESOLFT, SIM or localization-based approaches that do not rely on photoswitching, e.g. PAINT or DNA PAINT [5, 51]. Their use is more complicated once photoswitching by the dye itself is needed for superior resolution since photoswitching and the intramolecular healer often compete with each other for interactions with the triplet-state. Future studies will have to elaborate whether general design rules can be found for labelling antibodies, DNA or other targets in an optimal fashion to allow predictable photoswitching kinetics and also how the influence and damage of molecular oxygen can be removed.

4. Material and methods

4.1. Sample preparation and surface immobilization of oligonucleotides

Immobilization and the study of single fluorophores was achieved using a dsDNA scaffold comprising two 40-mer oligonucleotides, i.e. ssDNA-fluorophore and ssDNA-biotin. Sequences of both oligomers were adapted from the literature [49, 52, 53]. Single immobilized fluorophore molecules were studied in LabTek 8-well chambered cover slides (Nunc/VWR, The Netherlands) with a volume of 750 μl, as described previously [54]. After cleaning with 0.1% HF and washing with PBS buffer (one PBS tablet containing 10 mM phosphate buffer (pH 7.4), 2.7 mM potassium chloride, and 137 mM sodium chloride was dissolved in deionized water; Sigma-Aldrich, The Netherlands), each chamber was incubated with a mixture of 5 mg/800 μl BSA and 1 mg/800 μl BSA-biotin (Sigma Aldrich, The Netherlands) at 4 °C in PBS buffer overnight. After rinsing with PBS buffer, each chamber was incubated with a 0.2 mg·ml^{-1} solution of streptavidin for 10 mins and subsequently rinsed with PBS buffer.

The immobilization of dsDNA was achieved by a biotin-streptavidin interaction using pre-annealed dsDNA with the aim of observing single emitters for prolonged periods of time and allowing free rotation of the fluorophores. For this, 5–50 μl of a 0.1 mM solution of ssDNA-fluorophore or ssDNA-NPA-fluorophore (strand 1: ATTO647N/Cy5-(NPA)-C6-5′-TAA TAT TCG ATT CCT TAC ACT TAT ATT GCA TAG CTA TAC G-3′, see van der Velde *et al* [27] for synthesis) was mixed with the complementary ssDNA-biotin at the same concentration (strand 2: biotin-5′-CGT ATA GCT ATG CAA TAT AAG TGT AAG GAA TCG AAT ATT A-3′). For immobilization of dsDNA comprising STAR635P, STAR635P-NPAA, or Cy5-TX, we used an experimental strategy for proximal conjugation of NPAA/TX as described previously [32]. In the procedure, we used identical DNA sequences as for ATTO647N/Cy5 (see strand 1/2). Samples of dsDNA were generated by mixing strand 1 with 5′-STAR635P and strand 2 (called STAR635P); STAR635P-NPAA was obtained by mixing strand 1 with 5′-STAR635P and strand 2 with 3′-NPAA. STAR635P-labelled ssDNA with strand sequence one was obtained directly from IBA (Göttingen, Germany). Cy5-TX was obtained as described previously [32] by mixing strand 1 containing 5′-Cy5 and strand 2 with 3′-TX. Cy5-COT and the respective control was obtained with a different shorter dsDNA scaffold using P2 (Biotin-5′-CGT CCA GAG GAA TCG AAT ATT A-3′-NH_2) reacted to NHS-COT; see Smit *et al* [46] for details. Hybridizing this strand to ssDNA-Cy5 (Cy5-5′-TAA TAT TCG ATT CCT CTG GAC G-3′) gave the Cy5-COT sample.

Generally, mixtures of oligos were heated to 98 °C for 4 min and cooled down to 4 °C at a rate of 1 °C·min^{-1} in annealing buffer (500 mM sodium chloride, 20 mM Tris-HCL, and 1 mM EDTA at pH 8). The treated LabTek cover slides were incubated with a 50–100 pM solution of pre-annealed dsDNA for 1–2 min. All single molecule experiments were carried out at room temperature (22 °C ± 1 °C). Oxygen was removed from the buffer system with an oxygen-scavenging system (PBS, pH 7.4, containing 10% (wt/vol) glucose, 10% (vol/vol) glycerin, 50 mg ml^{-1} glucose-oxidase, and 100–200 μg ml^{-1} catalase). Glucose-oxidase catalase (GOC) [54, 55] was used instead of a combination of protocatechuic acid and protocatechuate-3,4-dioxygenase (PCA/PCD) [56] to avoid convolution of inter- and intramolecular photostabilization with PCA [57].

The procedures for the functionalization of oligonucleotides have been established before and described in detail in Smit *et al* [46].

4.2. Confocal scanning microscopy and data analysis

A custom-built confocal microscope, described previously [26], was used to study the fluorescence properties of organic fluorophores on the level of single molecules. Excitation was

achieved with a spectrally filtered laser beam from a pulsed supercontinuum source (SuperK Extreme, NKT Photonics, Denmark) with an acoustooptical tunable filter (AOTFnc-VIS, EQ Photonics, Germany), leading to 2 nm broad excitation pulses centred around 640 nm. The spatially filtered beam was coupled to an oil-immersion objective (60×, numerical aperture (NA) 1.35, UPLSAPO 60XO mounted on an IX71 microscope body, both from Olympus, Germany) by a dichroic beam splitter (zt532/642rpc, AHF Analysentechnik, Tuebingen, Germany). Surface scanning was performed using a XYZ-piezo stage with 100 × 100 × 20 μm range (P-517-3CD with E-725.3CDA, Physik Instrumente, Germany). Fluorescence was collected by the same objective, focused onto a 50 μm pinhole, and detected with an avalanche photodiode (τ-spad, <50 dark counts per second, PicoQuant, Germany) using appropriate spectral filtering (ET700/75 AHF, both from Analysentechnik). The detector signal was registered using a Hydra Harp 400 ps event timer and a module for time-correlated single-photon counting (both from PicoQuant). The data was evaluated using custom-made LabVIEW software [52, 53]. Blinking kinetics were extracted from fluorescent time traces in the form of on- and off-times according to established procedures [52]. Fluorescence lifetimes were determined using time-correlated single-photon counting as described previously [26].

4.3. Single molecule STED and confocal microscopy

ATTO647N and NPA-ATTO647N: Single molecule STED microscopy and the corresponding confocal microscopy were performed on a Microtime-200 STED microscope (PicoQuant, Berlin, Germany). Excitation was performed at 640 nm (LDH-D-C-640P laser diode, PicoQuant) and STED at 765 nm, at 10 MHz. A donut-shaped intensity distribution of the STED laser was realized by the easy-STED approach in which a $\lambda/4$ phase plate was inserted into the collimated STED beam, and was overlaid to the excitation beam using the appropriate filter (SBDC 565, AHF, Analysentechnik, Germany). Both the excitation and STED laser were focused into the sample through an oil-immersion objective (UPlanSapo 100×, NA 1.4, Olympus, Japan) mounted on an IX73 microscope body (Olympus, Germany) by dichroic beam splitter (ZT 640/752 rpc-UF3, Chroma, USA). Fluorescence was collected through the same objective and detected by avalanche photodiodes (Excelitas Technologies, Quebec, Canada) with corresponding spectral filtering (HQ 690/70, AHF Analysentechnik, Germany). The data was analysed with the Symphotime64 software (PicoQuant, Berlin, Germany). For fitting the point spread functions with a 2D Lorentzian and/or Gaussian function, a custom made ImageJ macro was used. The following 2D Gaussian function was used: $f(x,y) = a + bc^{-\frac{(x-d)^2+(y-e)^2}{2c^2}}$, and the following 2D Lorentzian function was used: $f(x,y) = a + b\frac{1}{\pi}\frac{\frac{1}{2}c}{(x-d)^2+(y-e)^2+(\frac{1}{2}c)^2}$ with a as background, b the amplitude, c the spread (sigma), d the x position and e the center position y.

STAR635P and STAR635P: STED microscopy images were obtained using a custom-built STED microscope setup equipped with synchronized pulsed lasers for fluorophore excitation and de-excitation based in the lab of Stefan Hell. The excitation laser beam at a wavelength of 637 nm was provided by a triggerable laser diode with a pulse duration of 120 ps (PicoQuant, Berlin, Germany). The STED laser pulses was obtained from a tunable Ti:sapphire laser with a repetition rate of 80 MHz and a pulse duration of 120 fs (Coherent LaserSystems GmbH, Dieburg, Germany). The STED laser was operated at a center wavelength of 750 nm and its pulses were stretched to 300 ps by coupling the STED beam into a 100 m polarization maintaining single mode optical fiber (Thorlabs GmbH, Munich, Germany) after guiding the beam through 30 cm of SF6 (dense flint) glass rods in order to prevent nonlinear effects in the fiber. The typical toroidal lateral intensity distribution used in STED microscopy was generated by guiding the STED beam through a vortex phase plate (RPC Photonics, Rochester, NY, USA). The STED laser pulses were used to trigger the excitation laser and the time delay between excitation and STED laser pulses was optimized for most efficient photophysical switching of fluorescent molecules. The excitation and STED laser beam paths were combined by a dichroic mirror (AHF Analysentechnik, Tuebingen, Germany). The beams were circularly polarized by using an adjustable quarter-wave retarder plate (Thorlabs GmbH, Munich, Germany) and then focused through a 100 × 1.4 NA oil objective (Leica Microsystems GmbH, Wetzlar, Germany). Images were recorded by resonant mirror scanning (15.8 kHz) along the first lateral axis and by stage scanning along the second lateral axis using a piezo stage (Physik Instrumente GmbH, Karlsruhe, Germany). During image recording, the sample was illuminated with excitation and STED laser powers of 30 μW and 200 mW (measured in a backfocal plane), respectively. The image pixel size was set to (20 × 20) nm² and the pixel dwell time was set to 100 μs/pixel. The obtained fluorescence signal was cleaned up by a (675/67) nm bandpass filter (AHF Analysentechnik, Tuebingen, Germany) and collected with a free-beam avalanche photodiode (Perkin Elmer, Fremont, CA, USA). The software package ImSpector (https://www.imspector.de) [58] was used for microscope hardware control, image acquisition and image recording.

4.4. STORM microscopy

Widefield TIRF imaging was performed on an inverted microscope (Olympus IX-71, UPlanSApo ×100 NA 1.49 Objective, Olympus, Germany) in a similar manner to that described previously [26]. Images were collected with a back-illuminated electron multiplying charge-coupled device camera (512 × 512 pixel, C9100-13, Hammamatsu, Japan) with matching filters and optics. To study the reactivation and STORM parameters, the sample was illuminated with a 375 nm or 405 nm laser after off-switching.

Individual fluorophores were detected in TIRF movies using a fixed threshold and discoidal averaging filter. The number of emitters as a function of time was fitted to a

mono-exponential decay to obtain the mean photobleaching or off-switching lifetime. To identify the reactivated fluorophores, a fixed threshold and discoidal averaging filter was used over the first n frames after initiation of illumination with both the excitation and UV light. For a typical experiment, five movies were recorded of a given condition, which was repeated on three different days. Fluorescent transients were extracted from the data by selecting a 3 × 3 pixel area (pixel size 160 nm) around the emitter and plotting the resulting mean fluorescence intensity in time. These fluorescent transients were then processed in home-written software to extract other photophysical parameters such as signal-to-noise ratio and count-rate.

Acknowledgments

This work was financed by an ERC Starting Grant (ERC-STG 638536—SM-IMPORT to TC). The Zernike Institute for Advanced Materials and the Centre for Synthetic Biology (University of Groningen) provided funding for purchasing a STED microscope. J H M v d V acknowledges the Ubbo-Emmius fund (University of Groningen) for a PhD stipend. T C was supported by the Center of Nanoscience Munich (CeNS), Deutsche Forschungsgemeinschaft within SFB863 (project A13), GRK2062 (project C03), LMUexcellent and the Center for integrated protein science Munich (CiPSM). We thank PicoQuant for experimental support and fruitful discussions. We thank D Griffith for corrections and thoughtful comments. We finally thank Stefan Hell and his laboratory, in particular Volker Westphal and Fabian Goettfert for support of this study.

ORCID iDs

Jochem H Smit https://orcid.org/0000-0002-3597-9429
Thorben Cordes https://orcid.org/0000-0002-8598-5499

References

[1] Rust M J, Bates M and Zhuang X 2006 Stochastic optical reconstruction miscroscopy (STORM) provides sub-diffraction-limit image resolution *Nat. Methods* **3** 793–5
[2] Heilemann M *et al* 2008 Subdiffraction-resolution fluorescence imaging with conventional fluorescent probes *Angew. Chem., Int. Ed.* **47** 6172–6
[3] Heilemann M, Van De Linde S, Mukherjee A and Sauer M 2009 Super-resolution imaging with small organic fluorophores *Angew. Chem., Int. Ed.* **48** 6903–8
[4] Betzig E *et al* 2006 Imaging intracellular fluorescent proteins at nanometer resolution *Science* **313** 1642–5
[5] Sharonov A and Hochstrasser R M 2006 Wide-field subdiffraction imaging by accumulated binding of diffusing probes *Proc. Natl Acad. Sci.* **103** 18911–6
[6] Hell S W and Wichmann J 1994 Breaking the diffraction resolution limit by stimulated emission: stimulated-emission-depletion fluorescence microscopy *Opt. Lett.* **19** 780–2
[7] Hell S W and Kroug M 1995 Ground-state-depletion fluorscence microscopy: a concept for breaking the diffraction resolution limit *Appl. Phys.* B **60** 495–7
[8] Hell S W 2003 Toward fluorescence nanoscopy *Nat. Biotechnol.* **21** 1347–55
[9] Hell S W 2008 Microscopy and its focal switch *Nat. Methods* **6** 24
[10] Hell S W *et al* 2015 The 2015 super-resolution microscopy roadmap *J. Phys. D: Appl. Phys.* **48** 443001
[11] Sahl S J and Moerner W 2013 Super-resolution fluorescence imaging with single molecules *Curr. Opin. Struct. Biol.* **23** 778–87
[12] Kasper R *et al* 2010 Single-molecule STED microscopy with photostable organic fluorophores *Small* **6** 1379–84
[13] Gordon M P, Ha T and Selvin P R 2004 Single-molecule high-resolution imaging with photobleaching *Proc. Natl Acad. Sci. USA* **101** 6462–5
[14] Qu X, Wu D, Mets L and Scherer N F 2004 Nanometer-localized multiple single-molecule fluorescence microscopy *Proc. Natl Acad. Sci. USA* **101** 11298–303
[15] Lidke K, Rieger B, Jovin T and Heintzmann R 2005 Superresolution by localization of quantum dots using blinking statistics *Opt. Express* **13** 7052–62
[16] Ram S, Ward E S and Ober R J 2006 Beyond Rayleigh's criterion: a resolution measure with application to single-molecule microscopy *Proc. Natl Acad. Sci. USA* **103** 4457–62
[17] Olivier N, Keller D, Gönczy P and Manley S 2013 Resolution doubling in 3D-STORM imaging through improved buffers *PLoS One* **8** e69004
[18] Olivier N, Keller D, Rajan V S, Gönczy P and Manley S 2013 Simple buffers for 3D STORM microscopy *Biomed. Opt. Express* **4** 885–99
[19] Dertinger T, Colyer R, Iyer G, Weiss S and Enderlein J 2009 Fast, background-free, 3D super-resolution optical fluctuation imaging (SOFI) *Proc. Natl Acad. Sci.* **106** 22287–92
[20] Liphardt B, Liphardt B and Lüttke W 1981 Laser dyes with intramolecular triplet quenching *Opt. Commun.* **38** 207–10
[21] Liphardt B and Lüttke W 1981 Laserfarbstoffe, I bifluorophore laserfarbstoffe zur steigerung des wirkungsgrades von Farbstoff-lasern *Liebigs Ann. Chem.* **1981** 1118–38
[22] Liphardt B, Liphardt B and Lüttke W 1983 Laser dyes III: concepts to increase the photostability of laser dyes *Opt. Commun.* **48** 129–33
[23] Altman R B *et al* 2012 Cyanine fluorophore derivatives with enhanced photostability *Nat. Methods* **9** 68–71
[24] Tinnefeld P and Cordes T 2012 Self-healing' dyes: intramolecular stabilization of organic fluorophores *Nat. Methods* **9** 426–7
[25] Blanchard S C 2012 Reply to 'Self-healing' dyes: intramolecular stabilization of organic fluorophores *Nat. Methods* **9** 427–8
[26] Van Der Velde J H M *et al* 2013 Mechanism of intramolecular photostabilization in self-healing cyanine fluorophores *ChemPhysChem* **14** 4084–93
[27] Van Der Velde J H M *et al* 2016 A simple and versatile design concept for fluorophore derivatives with intramolecular photostabilization *Nat. Commun.* **7** 1–15
[28] Zheng Q *et al* 2012 On the mechanisms of cyanine fluorophore photostabilization *J. Phys. Chem. Lett.* **3** 2200–3
[29] Zheng Q *et al* 2014 Ultra-stable organic fluorophores for single-molecule research *Chem. Soc. Rev.* **43** 1044–56
[30] Dave R, Terry D S, Munro J B and Blanchard S C 2009 Mitigating unwanted photophysical processes for improved single-molecule fluorescence imaging *Biophys. J.* **96** 2371–81

[31] Juette M F *et al* 2014 The bright future of single-molecule fluorescence imaging *Curr. Opin. Chem. Biol.* **20** 103–11
[32] Van Der Velde J H M *et al* 2015 Intramolecular photostabilization via triplet-state quenching: design principles to make organic fluorophores 'self-healing' *Faraday Discuss.* **184** 221–35
[33] Uno S *et al* 2014 Super-resolution imaging *Nat. Chem.* **6** 681–9
[34] Nanguneri S, Flottmann B, Herrmannsdörfer F, Thomas K and Heilemann M 2014 Single-molecule super-resolution imaging by tryptophan-quenching-induced photoswitching of phalloidin-fluorophore conjugates *Microsc. Res. Tech.* **77** 510–6
[35] Acuna G P *et al* 2012 Fluorescence enhancement at docking sites of DNA-directed self-assembled nanoantennas *Science* **338** 506–10
[36] Yuan H, Khatua S, Zijlstra P, Yorulmaz M and Orrit M 2013 Thousand-fold enhancement of single-molecule fluorescence near a single gold nanorod *Angew. Chem., Int. Ed.* **52** 1217–21
[37] Campos L A *et al* 2011 A photoprotection strategy for microsecond-resolution single-molecule fluorescence spectroscopy *Nat. Methods* **8** 143–6
[38] Guo J, Wang S, Dai N, Teo Y N and Kool E T 2011 Multispectral labeling of antibodies with polyfluorophores on a DNA backbone and application in cellular imaging *Proc. Natl Acad. Sci.* **108** 3493–8
[39] Marrocco M 2008 Two-photon excitation fluorescence correlation spectroscopy of diffusion for Gaussian–Lorentzian volumes *J. Phys. Chem.* A **112** 3831–6
[40] Blom H and Björk G 2009 Lorentzian spatial intensity distribution in one-photon fluorescence correlation spectroscopy *Appl. Opt.* **48** 6050
[41] Eggeling C *et al* 2009 Direct observation of the nanoscale dynamics of membrane lipids in a living cell *Nature* **457** 1159–62
[42] Danzl J G *et al* 2016 Coordinate-targeted fluorescence nanoscopy with multiple off states *Nat. Photon.* **10** 122
[43] Wurm C A *et al* 2012 Novel red fluorophores with superior performance in STED microscopy *Opt. Nanoscopy* **1** 1–7
[44] Cordes T *et al* 2010 Resolving single-molecule assembled patterns with superresolution blink-microscopy *Nano Lett.* **10** 645–51
[45] Vogelsang J *et al* 2010 Make them blink: probes for super-resolution microscopy *ChemPhysChem* **11** 2475–90
[46] Smit J *et al* 2018 On the impact of competing intra- and intermolecular triplet-state quenching on photobleaching and photoswitching kinetics of organic fluorophores (bioRxiv:371443) (https://doi.org/10.1101/371443)
[47] Vaughan J C, Jia S and Zhuang X 2012 Ultrabright photoactivatable fluorophores created by reductive caging *Nat. Methods* **9** 1181–4
[48] Vaughan J C, Dempsey G T, Sun E and Zhuang X 2013 Phosphine quenching of cyanine dyes as a versatile tool for fluorescence microscopy *J. Am. Chem. Soc.* **135** 1197–200
[49] Cordes T, Vogelsang J and Tinnefeld P 2009 On the mechanism of trolox as antiblinking and antibleaching reagent *J. Am. Chem. Soc.* **131** 5018–9
[50] Glembockyte V and Cosa G 2017 Redox-based photostabilizing agents in fluorescence imaging: the hidden role of intersystem crossing in geminate radical ion pairs *J. Am. Chem. Soc.* **139** 13227–33
[51] Jungmann R *et al* 2010 Single-molecule kinetics and super-resolution microscopy by fluorescence imaging of transient binding on DNA origami *Nano Lett.* **10** 4756–61
[52] Vogelsang J, Cordes T, Forthmann C, Steinhauer C and Tinnefeld P 2009 Controlling the fluorescence of ordinary oxazine dyes for single-molecule switching and superresolution microscopy *Proc. Natl Acad. Sci.* **106** 8107–12
[53] Vogelsang J, Cordes T and Tinnefeld P 2009 Single-molecule photophysics of oxazines on DNA and its application in a FRET switch *Photochem. Photobiol. Sci.* **8** 486–96
[54] Aitken C E, Marshall R A and Puglisi J D 2008 An oxygen scavenging system for improvement of dye stability in single-molecule fluorescence experiments *Biophys. J.* **94** 1826–35
[55] Vogelsang J *et al* 2008 A reducing and oxidizing system minimizes photobleaching and blinking of fluorescent dyes *Angew. Chem., Int. Ed.* **47** 5465–9
[56] Hu J and Zhang C Y 2013 Simple and accurate quantification of quantum yield at the single-molecule/particle level *Anal. Chem.* **85** 2000–4
[57] Le Gall A *et al* 2011 Improved photon yield from a green dye with a reducing and oxidizing system *ChemPhysChem* **12** 1657–60
[58] Schonle A 2006 *Imspector Image Acquisition & Analysis Software* (Goettingen: Abberior Instruments) *v.0.10* (www.imspector.de)